ARHGEF3 Regulates Hair Follicle Morphogenesis

Krithika Kalyanakrishnan[1-6], Amy Beaudin[1-6], Alexandra Jetté[1,5,6], Sarah Ghezelbash[7,8], Diana Ioana Hotea[1-6], Jie Chen[9-10], Philippe Lefrançois[7,8,11] and Mélanie Laurin[1-6]

Affiliations:

[1] Centre de recherche du CHU de Québec – Université Laval, axe Oncologie, Québec, Canada

[2] Programme de biologie moléculaire et cellulaire, Université Laval

[3] Département de biologie moléculaire, biochimie médicale et pathologie, Université Laval

[4] Faculté de médecine, Université Laval

[5] Centre de recherche sur le cancer de l'Université Laval (CRC)

[6] Centre de recherche en organogénèse expérimentale (LOEX)

[7] Cancer Axis, Lady Davis Institute for Medical Research, Montreal, QC, Canada

[8] Division of Experimental Medicine, McGill University, Québec, Canada

[9] Department of Cell & Developmental Biology, University of Illinois at Urbana-Champaign, Urbana, IL, USA

[10] Department of Biomedical and Translational Sciences, Carle Illinois College of Medicine, Urbana, IL 61801

[11] Division of Dermatology, Department of Medicine, McGill University, Montréal, QC, Canada.

Corresponding author's email address:

melanie.laurin@crchudequebec.ulaval.ca

Key words: morphogenesis, hair follicle, ARHGEF3, placode, RhoGEF, Rho GTPase, P-cadherin

ABSTRACT

During embryogenesis, cells arrange into precise patterns that enable tissues and organs to develop specialized functions. Despite its critical importance, the molecular choreography behind these collective cellular behaviors remains elusive, posing a major challenge in developmental biology and limiting advances in regenerative medicine. By using the mouse hair follicle as a mini-organ system to study the formation of bud-like structures during embryonic development, our work uncovers a crucial role for the Rho GTPase regulator ARHGEF3 in hair follicle morphogenesis. We demonstrate that *Arhgef3* expression is upregulated at the onset of hair follicle placode formation. In *Arhgef3* knockout animals, we observed defects in placode compaction, leading to impaired hair follicle downgrowth. Through cell culture models, we show that ARHGEF3 promotes F-actin accumulation at the cell cortex and P-cadherin enrichment at cell-cell junctions. Collectively, our study identifies ARHGEF3 as a new regulator of cell shape rearrangements during hair placode morphogenesis, warranting further exploration of its role in other epithelial appendages that arise from similar developmental processes.

INTRODUCTION

The molecular mechanisms that coordinate collective cell behaviors during organogenesis remain poorly understood. Hair follicles in mouse skin serve as ideal mini-organs for studying these processes due to their abundance, spatial pattern, and global alignment within the epidermal plane (1). During embryonic development, hair follicle progenitors are specified in the epidermis through paracrine and reciprocal signaling between the epidermal and underlying dermal compartments (2). Extensive loss- and gain-of-function experiments have elucidated the sequence of actions of key developmental pathways including BMP, WNT, SHH, and FGF that regulate hair follicle cell specification, downgrowth, and differentiation (3). More recent studies have also highlighted how mechanical forces influence and shape the architecture of the skin (4–9). Despite these significant advances, only a few downstream molecular effectors have been identified as crucial in mediating the effects of upstream signaling and mechanical input during hair follicle morphogenesis (10,11).

The development of the skin epidermis begins when cells from the surface ectoderm commit to an epidermal fate (3). By balancing proliferation and differentiation, these progenitors generate a stratified squamous epithelium, comprising an innermost proliferative basal cell layer and three differentiated keratinocyte layers, which are critical for the skin's barrier function (12). Additionally, some of these progenitors give rise to skin appendages, such as the hair follicles (13). The first distinct morphological sign of hair follicle development is the formation of an epithelial thickening known as the hair placode. Directional cell migration and cell compaction have been shown to promote placode formation (14). Following the elongation of placode cells, external contractile forces in both the epidermal and dermal compartments cause these cells to expand their basal surface while the apical surface remains unchanged, which promotes their invagination (7). As remodeling of the extracellular matrix occurs around the placode, the pressure on placode cells is reduced, facilitating their reentry into mitosis (7). Further downgrowth of the bud is achieved through oriented cell divisions, leading to the formation of hair germs and hair pegs (7,15). Genetic manipulations, such as the loss of Myosin IIa (*Myh9* knockout mice) or treatment of mouse embryos with inhibitors of actomyosin remodeling, have highlighted the crucial role of cytoskeletal components in these processes (7,10,11,14,16,17).

In mouse skin, the alignment of hair follicles along the anterior-posterior axis of the embryo and the polarization of their downgrowth are governed by planar cell polarity (PCP), which refers to the coordinated polarization of a field of cells within a tissue plane (18,19). As the epidermis develops,

76 significant changes occur in the shape and orientation of basal cells (10,20). These changes coincide with
77 and are essential for the partitioning of PCP proteins, such as CELSR1, along the anterior-posterior axis
78 of the basal cells. Disruption of epidermal contractility perturbs the establishment of PCP cues in the
79 epidermis and leads to the misorientation of hair follicles (10,20). Importantly, mutations in conserved
80 PCP components, such as *Frizzled-6*, *Celsr1* and *Vangl2,* result in misalignment of developing hair
81 follicles (19,21–24). Still, the molecular effectors that act downstream of these core PCP components to
82 coordinate cell rearrangements in the hair follicle remain to be identified. Understanding how PCP is
83 established in skin is vital for comprehending how polarity is coordinated among neighboring cells and
84 how it is manifested at tissue level.

85 In addition to the signals provided by epidermal cells, proper hair follicle morphogenesis requires
86 extensive cellular rearrangements within the developing hair follicle. In the placode, counter-rotational
87 cell movements play a crucial role in ensuring the polarization of the hair follicle and the asymmetric
88 positioning of progenitor cells (16). These rearrangements are reminiscent of convergent extension
89 movements, which promote directional elongation via cell intercalation and junctional shrinkage
90 (16,25,26). While PCP components could help bias junctional contraction in one direction, another
91 mechanism proposed for facilitating cell movement and neighbor exchange in the placode is the
92 upregulation of the adherens junction component P-cadherin (also known as Cadherin-3) and the
93 concurrent downregulation of E-cadherin in the central cells of the placode (27–29). Following rotational
94 movements, P-cadherin-enriched cells become positioned in the anterior region of the polarized hair
95 follicle, while E-Cadherin remains downregulated (16,19). This transition is crucial, as overexpression
96 of E-cadherin can inhibit hair follicle formation by preventing invagination (27,30). Again, the molecular
97 mechanisms downstream of these adherens junctions that contribute to hair follicle morphogenesis
98 remain poorly understood.

99 Recently, we utilized our ability to transduce epidermal progenitors by injecting lentiviral particles into
100 the amniotic cavities of mouse embryos using ultrasound guidance (31). This method allowed us to
101 conduct an RNAi-mediated screen to identify new regulators of epidermal and hair follicle
102 morphogenesis among components of the Rho GTPase networks, which are key cytoskeletal regulators
103 (32–35). One of the candidates identified is ARHGEF3, also known as XPLN (36,37). Our findings
104 revealed that cells transduced with shRNAs targeting ARHGEF3 failed to contribute to hair follicles,
105 although their representation in the epidermis remained unchanged (32). This suggests that ARHGEF3

106 is a positive regulator of hair follicle development but is not essential for the formation of the epidermal
107 barrier.
108
109 ARHGEF3 functions as a RhoGEF for RHOA and RHOB via its DH-PH GEF domain (36). In addition
110 to its GEF activity, ARHGEF3 acts as a negative regulator of mTORC2, inhibiting signaling to AKT and
111 restricting myoblast differentiation (38). In injured muscles, ARHGEF3 operates differently in a RHOA-
112 dependent manner to restrict muscle regeneration. Remarkably, muscles in *Arhgef3*$^{-/-}$ knockout animals
113 repair more effectively through the activation of autophagy (39). Another *Arhgef3*-null mouse model
114 revealed that depletion of this RhoGEF leads to larger platelets without impairing their function (40). In
115 a disease context, ARHGEF3 has been shown to promote the stability of ACLY, an ATP citrate lyase, by
116 preventing its association with the E3 ligase NEDD4 in lung cancer cells (41). Despite these findings,
117 the biological and molecular functions of ARHGEF3 remain largely unexplored. Here, we examine how
118 ARHGEF3 regulates hair follicle morphogenesis by modulating cell compaction and P-cadherin-
119 mediated cell-cell junctions.

RESULTS

ARHGEF3 is expressed in the developing skin.

Of the 26 potential regulators of hair follicle morphogenesis identified in our screen, *Arhgef3* was the only one found to be differently expressed between the hair placodes and the interfollicular epidermis across multiple studies (29,32,42–45). Indeed, analysis of transcriptomic datasets from the *Hair-GEL* and *Sulic et al.* platforms revealed that *Arhgef3* mRNA levels were 2.57 times higher in the hair placodes compared to the epidermis (**Fig. 1A**) (44–46). Using these datasets, isoform switch analysis revealed that *Arhgef3* transcript variant 3, (*ENSMUST000000224981.2; NM_001289687.1*) was the most highly expressed isoform in the skin (**Fig. 1B**). Furthermore, the difference in gene expression between the placode and epidermis persisted when examining this specific transcript (**Fig. 1B**). To investigate whether this differential expression was observable directly in mouse skin tissue, we employed *in situ* hybridization on E18.5 mouse skin sections using a fluorescently labeled *Arhgef3* probe. Our results confirmed that *Arhgef3* mRNA levels were significantly higher in the hair placode compared to the epidermis, and this elevated expression of *Arhgef3* persisted in the developing hair follicle throughout its growth (**Fig. 1C**). This difference in expression between the two compartments was further appreciated when we compared it to the broad distribution of the ubiquitously expressed *Polr2a* mRNA in the same tissue (**Fig. 1C**). In summary, the upregulation of *Arhgef3* expression at the onset of hair follicle development suggests that it may play a crucial role during its morphogenesis.

ARHGEF3 is not required for skin barrier formation.

To examine the role of *Arhgef3* during skin development, we employed an *Arhgef3*-knockout mouse strain (*Arhgef3*$^{-/-}$), generated by deleting a portion of exon 3, which is the first exon common to all four *Arhgef3* isoforms in mice (39). *Arhgef3-null* animals are viable, fertile, and exhibit enhanced muscle repair capabilities following injury, but their skin has not been thoroughly characterized (39). In our screen, the proportion of cells that expressed shRNAs targeting *Arhgef3* were not enriched or depleted in the epidermis at endpoint, which was similar to the behavior of cells expressing non-targeting shRNAs (32). This result suggests that ARHGEF3 is not crucial for epidermal development. However, because shRNA-mediated depletion can result in partial knockdown of their target and since ARHGEF3 has been shown to regulate the proliferation of other cell types (41,47), we investigated if the complete loss of ARHGEF3 in knockout embryos impairs epidermal proliferation. To explore this, pregnant females were pulsed with 5-ethynyl-2'-deoxyuridine (EdU) to label the cells in S-phase in the embryos. When

152 quantifying the number of EdU^+ basal cells, which are labelled by P-cadherin, we observed a slight
153 decrease in their average number in *Arhgef3*$^{-/-}$ embryos compared to wild-type animals (**Fig. 2A, B**).
154 Nevertheless, this difference was not statistically significant. Furthermore, measuring epidermal
155 thickness using immunofluorescence for P-cadherin to identify the base of the epidermis revealed no
156 significant differences between knockout and wild-type animals (**Fig. 2C, D**). Immunofluorescence
157 analysis also revealed that embryos from both genotypes showed comparable levels of Keratin 10, a
158 marker of differentiated suprabasal cells in the epidermis (**Fig. 2C**). Likewise, levels of LORICRIN and
159 Filaggrin, predominantly expressed in the granular layer of the epidermis, remained unchanged in the
160 absence of ARHGEF3 (**Fig. 2E, F**). Finally, we conducted a barrier assay from E16.5 to E18.5 in wild-
161 type and *Arhgef3* knockout embryos and observed normal, development of the skin barrier in all animals
162 (**Fig. 2G**). Collectively, these analyses indicate that ARHGEF3 is dispensable for epidermal
163 development, which is consistent with the findings from our screen (32).
164
165 **ARHGEF3 is required for hair follicle morphogenesis.**
166 With the confirmation that disrupting ARHGEF3 expression does not result in widespread epidermal
167 defects, we proceeded to investigate whether this RhoGEF is essential for proper hair follicle
168 development, as indicated by our screen (32). First, we assessed whether ARHGEF3 is required for the
169 specification and initiation of hair follicle development. For this purpose, we used whole-mount
170 immunofluorescence of P-cadherin on E16.5 back skin, which allowed us to visualize hair placodes,
171 germs, and pegs from the staggered hair follicle waves (**Fig. 3A**). Quantitative analysis of these structures
172 showed no significant difference in their average number between control and *Arhgef3*-null samples (**Fig.
173 3B**). To determine if the complete loss of ARHGEF3 affects cell proliferation in the hair follicle, we
174 performed an EdU pulse experiment. Although there was a slight reduction in the number of EdU^+ hair
175 follicle cells in *Arhgef3*$^{-/-}$ embryos, this decrease was minimal and unlikely to have a significant impact
176 on hair follicle morphogenesis. This was further supported by the quantification of hair peg length, which
177 showed no significant difference between their average lengths in control and *Arhgef3*$^{-/-}$ embryos (**Fig.
178 3E**). Therefore, ARHGEF3 does not play a role in hair follicle specification and initiation.
179
180 As hair follicles develop in mice, they typically align along the anterior-posterior axis of the embryo and
181 penetrate the dermis at an angle relative to the basement membrane, rather than perpendicularly (19). In
182 wild-type embryos, we measured that the hair follicles downgrowth within the dermis is evenly
183 distributed around an average angle of 63 degrees relative to the basement membrane (**Fig. 3F, G** green

184 line). Interestingly, *Arhgef3*-null hair follicles displayed a different distribution of angles around the
185 increased average of 67 degrees (**Fig. 3G**; green line). In fact, we observed a significant increase in the
186 percentage of straight-growing hair follicles in *Arhgef3*$^{-/-}$ embryos compared to the wild-type animals
187 (**Fig. 3G**, dash bin in both genotypes), although their orientation along the anterior-posterior plane
188 remained largely unchanged as observed in figure 3A. This resulted in a more entangled hair coat in
189 shaved adult *Arhgef3*$^{-/-}$ animals, as the hair that fell away remained in clumps. This contrasted with the
190 wild-type coat, in which individual hairs were easily dispersed.
191
192 PCP, which refers to the polarization of cells within the plane of an epithelium, is essential to the
193 asymmetric downgrowth and alignment of hair follicles along the anterior-posterior plane of mice. As
194 the skin develops, the progressive partitioning of core PCP components such as CELSR1 in epidermal
195 cells provides instructive cues for hair follicle polarization (19). Using whole-mount
196 immunofluorescence of CELSR1 and E-cadherin on E15.5 tissue, we investigated whether PCP is
197 established in the absence of ARHGEF3, which could explain the defect in hair follicle downgrowth
198 (**Fig. 4A**). First, we quantified the percentage of planar polarized cells, defined as cells with two opposing
199 domains of CELSR1 at their cell surface membrane (10). On average, the percentage of these cells was
200 similar in both *Arhgef3* knockout and wild type embryos (**Fig. 4A, B**). Quantification of the angle of
201 polarization also showed that it was the same along the anterior-posterior axis of the embryos (**Fig. 4A,**
202 **C**). These results suggest that CELSR1 domains are established in the epidermis of *Arhgef3* knockout
203 animals and that the hair follicle angling defects observed in *Arhgef3*-null animals are likely uncoupled
204 from the establishment of PCP in the epidermis.
205
206 **ARHGEF3 regulates P-cadherin mediated junctions.**
207 Having established that CELSR1 domains are present in the epidermis at the onset of hair follicle
208 development, we turned to a cell culture model of human keratinocytes (Ker-CT) to investigate the
209 consequence of increasing the level of *Arhgef3* expression on cellular architecture and gain insights into
210 the roots of the hair follicle defects. RT-qPCR analysis revealed that *ARHGEF3* mRNA is expressed in
211 proliferating keratinocytes (Day 0) and remains consistently expressed throughout calcium-induced
212 differentiation (Days 1 to 7) in culture (**Fig. 5A**). The differentiation of keratinocytes was confirmed by
213 measuring the expression of *Keratin 10 (KRT10)* and *LORICRIN* mRNA, as both epidermis markers
214 increase during differentiation (**Fig. 5A**). To mimic the increase in *Arhgef3* expression observed at the
215 onset of placode formation, we generated a 3xFLAG-ARHGEF3 (3xF-ARHGEF3) doxycycline-

216 inducible cell line by transducing a population of keratinocytes. Western blot analysis confirmed that the
217 fusion protein was only expressed upon doxycycline exposure (**Fig. 5B**). Immunofluorescence showed
218 that 3xF-ARHGEF3 localized to both the cytoplasm and nucleus in proliferating and differentiating
219 keratinocytes (**Fig. 5C**). We then investigated the impact of increased ARHGEF3 levels on keratinocytes
220 cell-cell junctions. In the presence of calcium, keratinocytes typically form E-cadherin-mediated cell-
221 cell junctions that display a distinct honeycomb pattern. This pattern was observed in wild-type
222 keratinocytes treated with doxycycline as well as in control 3xF-ARHGEF3 keratinocytes without
223 doxycycline (**Fig. 5D**). When 3xF-ARHGEF3 was overexpressed, the effect on E-cadherin at the junction
224 was modest. Although there was no significant enrichment or depletion of E-cadherin at the junction,
225 ARHGEF3-overexpressing cells exhibited more continuous and less tortuous (*zipper-like*) E-cadherin
226 staining at the cell-cell junction. Given that placode cells depend heavily on P-cadherin-mediated
227 adherens junctions, we investigated its localization in our keratinocyte populations. Under control
228 conditions, P-cadherin was evenly distributed at the cell-cell junctions between keratinocytes.
229 Remarkably, we observed that an increase in ARHGEF3 expression was associated with a significant rise
230 in P-cadherin levels at these junctions (**Fig. 5E**). This was particularly striking when looking at
231 orthogonal views, which also revealed an increase in the cell height of ARHGEF3-overexpressing
232 keratinocytes. To assess whether the observed rise in P-cadherin at the cell junctions was due to higher
233 protein expression levels, we conducted Western blot analysis. Although both E-cadherin and P-cadherin
234 levels increased during differentiation, no significant difference was detected between control and A
235 ARHGEF3-overexpressing cells. This suggests that the strong recruitment of P-cadherin to cell junctions
236 is not linked to an increased in its total protein levels (**Fig. 5F**). Therefore, ARHGEF3 appears to facilitate
237 the relocalization of P-cadherin to cell-cell junctions in keratinocytes without altering its overall
238 expression.
239
240 **ARHGEF3 regulates placode compaction.**
241 The formation of cell-cell junction between keratinocytes is typically associated with the recruitment of
242 F-actin at the junction and the formation of radial actin fibers, which could be observed in wild-type and
243 control keratinocytes (**Fig. 6A**). However, ARHGEF3 overexpression caused a notable accumulation of
244 F-actin at the cell cortex in keratinocytes, leading to cell compaction (**Fig. 6A**). This compaction was
245 characterized by an increase in cell height, as seen in orthogonal views. Remarkably, in some clusters of
246 ARHGEF3-overexpressing cells, keratinocytes appeared to stack on top of each other, a behavior not
247 observed in control condition at this time point (**Fig. 6A**, right panel). Importantly, this multilayering was

248 not due to premature differentiation, as these cells did not express the differentiation markers Keratin 10,
249 24 and 48 hours after the calcium switch (data not shown). This phenotype is strikingly similar to the cell
250 compaction and cell elongation observed in hair placodes, which is driven by centripetal migration. To
251 investigate whether defects in placode morphogenesis might explain the hair follicle phenotype observed
252 in *Arhgef3*$^{-/-}$ animals, we analyzed placode formation using whole-mount immunofluorescence for P-
253 cadherin on E16.5 back skin tissue. Consistent with previous studies, placode formation was associated
254 with an increase in P-cadherin, in both wild-type and *Arhgef3*-null embryos (**Fig. 6B**). Since placode
255 development is characterized by cell compaction, we measured the surface area of developing placodes
256 using P-cadherin staining. Our measurements revealed that the average surface area of placodes was
257 larger in *Arhgef3*-null animals (**Fig. 6C**). This suggests that increased *Arhgef3* expression at the onset of
258 placode formation aids in the morphogenesis of placodes. Conversely, insufficient *Arhgef3* expression
259 impairs hair follicle polarization, leading to a higher percentage of hair follicles growing straight.

260 **DISCUSSION**

261 Building on our morphogenesis screen and transcriptomic data showing elevated ARHGEF3 expression
262 in the placode relative to the epidermis, our study identified ARHGEF3 as a novel regulator of hair
263 follicle morphogenesis (32,44,45). Although few studies have investigated ARHGEF3 regulation in
264 mammalian cells, existing research shows that its expression is induced in muscles following their injury
265 or in microglia after LPS treatment to mimic inflammation (39,48). Additionally, TGFß1 downregulates
266 ARHGEF3, while HDAC inhibitors upregulate its expression in lung fibroblasts (41,49). Still, these
267 findings provide limited clues into how ARHGEF3 is regulated during skin development.
268
269 Interestingly, studies on the Xenopus orthologue, *Arhgef3.2*, offer valuable insights. Arhgef3.2 plays a
270 critical role in gastrulation, as demonstrated by loss- and gain-of-function experiments (50). In Xenopus,
271 BMP4 restricts cell movement by inhibiting Arhgef3.2 transcription, while BMP inhibition promotes its
272 expression (50,51). This is particularly intriguing given that BMP gradients in the epidermis also
273 influence hair follicle formation—with high BMP levels inhibiting hair follicle development, and low
274 BMP levels allowing placode initiation, which coincides with increased ARHGEF3 expression (2,3).
275 This suggests a conserved regulatory mechanism across species, where an inverse relationship between
276 BMP signaling and *Arhgef3* expression may be crucial for tissue morphogenesis.
277
278 The similarity between hair follicle morphogenesis and gastrulation is further underscored by the role of
279 convergent extension cell movements in both processes. During Xenopus gastrulation, BMP inhibits
280 convergent extension, while Arhgef3.2 regulates this process by interacting with Dsh2 via DAAM, two
281 components of the non-canonical WNT/PCP signaling pathway, which is essential for convergent
282 extension (50,52). Similarly, in hair follicle morphogenesis, PCP proteins are crucial not only for
283 providing instructive cues from the epidermis but also for coordinating cellular movements within the
284 developing hair follicle (16,19). These movements resemble convergent extension and are necessary for
285 proper hair follicle polarization. While it remains unclear if ARHGEF3 functions downstream of Dsh2
286 in mammalian cells, our data suggest that ARHGEF3 acts either downstream or independently of core
287 PCP cues in the skin, as these cues appear to be properly established in our system.
288
289 The collective behavior of cells depends heavily on the remodeling of cell-cell junctions. In hair follicles,
290 this process is partly controlled by the upregulation of P-cadherin and the downregulation of E-cadherin
291 (30,53). Our data suggest that while ARHGEF3 does not alter the overall levels of these adherens junction

292 components in keratinocytes, increased ARHGEF3 levels significantly enhance P-cadherin accumulation
293 at cell-cell junctions, with minimal impact on E-cadherin. Unraveling the molecular mechanisms that
294 allow ARHGEF3 to selectively promote P-cadherin localization will be an exciting direction for future
295 research. Currently, ARHGEF3's known protein partners are limited, and expanding its interactome will
296 likely deepen our understanding of its role in skin biology. Although ARHGEF3 exhibits both GEF-
297 dependent and GEF-independent functions, its role in increasing F-actin accumulation at the cellular
298 cortex of keratinocytes likely involves its RhoGEF activity. However, it remains unclear whether all
299 ARHGEF3's contributions to skin development depend solely on its ability to activate RHOA and
300 RHOB.
301
302 While our research has primarily centered on ARHGEF3's role in the epidermis and hair follicles, it is
303 important to note that hair follicle polarization and progenitor cell asymmetry also rely on dermal
304 contributions (7,16). Given that we employed a full knockout mouse model, the observed phenotypes
305 could potentially be influenced by dermal signaling (39). However, no significant abnormalities were
306 detected in the dermal cell population, and ARHGEF3 overexpression in keratinocytes resulted in cell-
307 autonomous effects, such as F-actin accumulation at the cell cortex and P-cadherin relocalization at the
308 membrane. To precisely address the role of dermal cells, developing an ARHGEF3 conditional mouse
309 model would be invaluable and could help broaden our understanding of ARHGEF3 biological functions.
310 Our findings highlight ARHGEF3 as a key regulator of hair follicle morphogenesis, linking it to
311 conserved pathways governing placode formation and junctional remodeling via BMP gradients. Given
312 the placode's central role in various epithelial appendages, future studies will be essential to further
313 explore ARHGEF3's broader functions in these developmental processes.

314 **MATERIALS AND METHODS**

315

316 **Animals models**

317 *Arhgef3*$^{-/-}$ mice were previously generated and described (39). Animals were rederived upon their arrival
318 at the CHU de Québec – Université Laval research center, where they are now maintained in a mouse-
319 specific pathogen-free (SPF) facility. All mouse experiments were approved by Université Laval Animal
320 Care Protection Committee, and they followed the Canadian Council of Animal Care Guidelines.

321

322 **RNA-Seq analysis**

323 Whole-genome RNA-sequencing data of a total of 9 placode-enriched and 9 interfollicular epithelium
324 (IFE) samples from E14.5 mice was collected from the *Hair-GEL* platform (2 placode-enriched and IFE
325 sample pairs, Gene Expression Omnibus accession number GSE70288), and *Sulic et al*. (7 placode-
326 enriched and IFE sample pairs, Gene Expression Omnibus accession number GSE212652). Raw fastq
327 files were quality-checked with FastQC. Transcript-level quantification was obtained with Salmon
328 (https://www.ncbi.nlm.nih.gov/pmc/articles/PMC5600148/) using selective alignment against the mm39
329 reference genome and transcriptome. Gene- and transcript-level fragments per kilobase per million
330 (FPKMs) were extracted using the IsoformSwitchAnalyzeR R package
331 (https://pubmed.ncbi.nlm.nih.gov/30989184/) and plotted using GraphPad Prism 10.

332 **RNAscope *in situ* hybridization**

333 RNAscope *in situ* hybridization (ISH) was performed using the RNAscope Multiplex Fluorescent V2
334 Assay (Advanced Cell Diagnostics, 323270) according to the manufacturer's protocol. Briefly, back skin
335 from E18.5 embryo was dissected, fixed with 4% PFA for 1 hour at 4°C, washed several times with 1X
336 PBS, and dehydrated in 20% sucrose overnight. The next day, the skin tissue was embedded and frozen
337 in Tissue Plus O.C.T. Compound Clear (Fisher Scientific, 4585). Skin sections of 14 µm were generated,
338 baked 30 minutes at 60°C, and fixed for 15 min at 4°C with 4% PFA. The sections were then dehydrated
339 with serial incubations in increasing concentrations of ethanol (50%, 70%, 100% twice), treated with
340 H_2O_2 for 10 minutes at room temperature, and with Protease IV (Advanced Cell Diagnostics, 322336)
341 for 30 min at room temperature. Subsequent hybridizations (*Arhgef3* or *Polr2a* probes, 2 hours at 40°C)
342 and amplifications (Amp1 (30 min, 40°C), Amp2 (30 min, 40°C) and Amp3 (15 min, 40°C)) were
343 alternated with washes (twice, 2 min at room temperature) with 1X washing buffer (Advanced Cell
344 Diagnostics, 310091). Both probes were in the C1 channel and fluorescence was developed using the
345 HRP-C1 reagent, followed by TSA Vivid Fluorophore 570 (Advanced Cell Diagnostics, 323272;

346 1:2,000) and HRP blocker. Sections were counterstained with DAPI (Advanced Cell Diagnostics,
347 320858), mounted using Invitrogen™ ProLong™ Diamond Antifade Mounting media (ThermoFisher,
348 P36970), and captured using an LSM-900 confocal microscope (Zeiss) with a LD C-Apochromat 40x
349 water immersion objective (NA: 1.1). Basic image adjustments were performed in Fiji (ImageJ).
350
351 **Immunofluorescence, microscopy, and image processing**
352 For whole-mount immunofluorescence on back skin tissues, embryos were fixed for 1 hour using 4%
353 PFA at room temperature. The embryos were washed several times in 1X PBS while gently shaking and
354 left to wash overnight. The following day the skin was dissected and blocked in gelatin buffer (1X PBS
355 supplemented with 2.5% normal donkey serum (Sigma, 566460), 1% BSA (Wisent, 800-095-EG), 2%
356 gelatin from cold water fish skin (Sigma, G7765) and 0.3% Triton X-100 (BioShop, TRX506.100) for at
357 least 2 hours with agitation at room temperature. For whole-mount CELSR1 staining, the gelatin blocking
358 buffer contained 2.5% fish gelatin, 2.5% normal donkey serum, 2.5% normal goat serum (Sigma,
359 NSO2L), 0.5% BSA and 0.1% Triton X-100 in 1X PBS and the washes were done using 0.1% Triton X-
360 100 in 1X PBS. Primary antibodies (see below) were diluted in gelatin buffer and incubated with agitation
361 overnight at 4ºC. The next day, the skin was washed 5 times with 0.3% Triton X-100 in 1X PBS.
362 Secondary antibodies were diluted in gelatin buffer and incubated overnight with agitation at 4ºC. The
363 following day, the back skin was washed with 0.3% Triton X-100 in 1X PBS for more than 3 hours
364 changing the solution at least 3 times, and then incubated with DAPI (Sigma, D9542; 0.2µg/ml) for 20
365 minutes. The nuclear stain was washed with 1X PBS followed by dH_2O after which tissues were mounted
366 on slides using Invitrogen™ ProLong™ Diamond Antifade Mounting media (ThermoFisher, P36970).
367 Primary antibodies were used as follows: P-cadherin (Cadherin-3, R&D, AF761; 1:400), E-cadherin
368 (R&D, AF748; 1:300) and CELSR1 (Fuchs lab gift, rabbit; 1:300). Secondary antibodies were used as
369 follows: donkey anti-goat IgG cross-adsorbed Alexa Fluor 488 (ThermoFisher, A11055; 1:200) and
370 donkey anti-rabbit IgG cross-adsorbed Alexa Fluor 594 (ThermoFisher, A21207; 1:200).
371
372 For immunofluorescence on cryosections, the back skin of embryos was fixed with 4% PFA for 1 hour
373 at 4ºC, washed several times with PBS 1X, and dehydrated in 20% sucrose overnight. The next day, the
374 skin tissues were embedded and frozen in Tissue Plus O.C.T. Compound Clear (Fisher Scientific, 4585).
375 Sections were fixed for 10 minutes in 4% PFA at room temperature, washed several times with PBS 1X,
376 and blocked using gelatin buffer for 1 hour. Sections were incubated with primary antibodies diluted in
377 gelatin buffer overnight at 4ºC. The next day, sections were washed with 0.3% Triton X-100 and

incubated with a secondary antibody (1:500) diluted in gelatin buffer for 1 hour. Later, these sections were washed with 0.3% Triton X-100, incubated with DAPI for 10 minutes and washed with PBS 1X. Sections were mounted using Invitrogen™ ProLong™ Diamond Antifade Mounting media. Primary antibodies were used as follows: P-cadherin (Cadherin-3, R&D, AF761; 1:400), Keratin 10 (BioLegend, 905403; 1:1,000), LORICRIN (BioLegend, 905104; 1:500) and FILAGGRIN (BioLegend, 905804; 1:400).

For immunofluorescence on Ker-CT, $1x10^5$ cells were plated in 15mm CultureWell™ (ThermoFisher, C24776). Cells were fixed for 15 minutes using 4% PFA at room temperature and washed several times in 1X PBS. Next, cells were blocked in blocking buffer (1X PBS supplemented with 2.5% normal donkey serum, 1% BSA and 0.1% Triton X-100) for 1 hour with agitation at room temperature. Primary antibodies (see below) were diluted in blocking buffer and incubated overnight at 4ºC. The next day, cells were washed once with 0.3% Triton X-100 in 1X PBS and twice with 1X PBS. Secondary antibodies (see below) were diluted in blocking buffer and incubated for 1 hour with agitation at room temperature. Cells were washed 3 times with 1X PBS and incubated for 10 minutes in 1X PBS containing DAPI. Cells were mounted on slides using Invitrogen™ ProLong™ Diamond Antifade Mounting media. Primary antibodies were used as follows: P-cadherin (Cadherin-3, R&D AF761; 1:400), E-cadherin (R&D AF748; 1:300) and FLAG-M2 (Sigma, F1804; 1:1,000). Secondary antibodies were used as follows: donkey anti-goat IgG cross-adsorbed Alexa Fluor (ThermoFisher, A11058 (594), A21447 (647); 1:1,000) and donkey anti-mouse IgG cross-adsorbed Alexa Fluor 488 (ThermoFisher, A-21202; 1:1,000). Phalloidin-iFluor 647 (Abcam, ab176759; 1:1,000) was used to label F-actin.

Images of whole-mounts, cryosections, and cells were captured using an LSM-900 confocal microscope (Zeiss) with either a Plan-Apochromat 20x air objective (NA: 0.8) or a LD C-Apochromat 40x water immersion objective (NA: 1.1). Basic image adjustments were performed in Fiji (ImageJ).

Quantification of cell proliferation and hair follicle length

For cell proliferation assay, pregnant female mice were injected intraperitoneally with 5-ethynyl-2'-deoxyuridine (EdU, Sigma, 900584), allowing E18.5 embryos to be pulsed for 30 minutes. Embryos were dissected and the back skin was embedded in OCT as described above. EdU detection on cryosections was done according to the manufacturer's instructions (Click-iT EdU Alexa Fluor 647 Imaging kit, Life Technologies, C10340). The ratio of EdU^+ cells to all cells ($DAPI^+$) was calculated for

410 basal (based on P-cadherin$^+$) and hair follicle (based on morphology) cells. To assess hair follicle length,
411 the same cryosections were analyzed by drawing a line (straight or segmented) from the bottom of the
412 basal layer until the end of the hair follicle and measured using Fiji (ImageJ).
413
414 **Quantification of hair follicle orientation and planar polarized cells**
415 To assess hair follicle orientation, cryosections of E18.5 back skin were stained with P-cadherin to
416 highlight the hair follicles and the basal layer in contact with the basement membrane. The angle between
417 the basal layer and the hair follicle was drawn and calculated using Fiji angle tool as depicted in Figure
418 3. An angularity of more than 80° was classified as a straight hair follicle. To evaluate if PCP is
419 established in the epidermis, CELSR1 and E-cadherin whole-mount immunofluorescence on E15.5 back
420 skin was performed and 3 regions of 75 x 75 µm were analyzed per embryo. PCP-polarized epidermal
421 cells were defined as cells in which opposing domains of CELSR1 were present. The frequency of the
422 angle of these domains relative to the anterior-posterior axis of the embryo was determined using the Fiji
423 straight-line tool.
424
425 **Barrier assay**
426 Briefly, E16.5, E17.5 and E18.5 embryos were isolated from the pregnant mother. Euthanized embryos
427 were immersed in ice-cold PBS 1X for 30 min. Embryos were immersed in a cold methanol gradient (1–
428 25%, 2–50%, 3–75%, 4–100% methanol) in water, and rehydrated in a methanol gradient in water (1–
429 75%, 2–50%, 3–25%, 4–0% methanol), taking 2 minutes per step. Embryos were next immersed in 0.1%
430 toluidine blue solution in water on ice for 2 minutes, with inversions. Embryos were destained in PBS
431 1X at least twice to reveal the dye pattern and barrier properties.
432
433 **Keratinocyte cell culture and cell differentiation assay**
434 Ker-CT, an hTERT-immortalized keratinocyte cell line isolated from the foreskin of a male patient, was
435 obtained from ATCC (CRL-4048). Cells were maintained as recommended in KGM™ Gold BulletKit™
436 media (Lonza, 192060) in a 37°C incubator in the presence of 5% CO_2. For differentiation assay, $4x10^5$
437 cells were plated in 9.6 cm^2 wells. Differentiation was induced 24 hours following plating, when cells
438 reached 80% confluency. For this, growth media was removed and replaced with KGM containing 1.5
439 mM of $CaCl_2$ without growth factors. Total RNA was collected at 0-, 2-, 3- and 7-days following
440 differentiation for further analyses.
441

442 **RNA isolation and RT-qPCR**

443 RNA isolation was achieved using the Invitrogen™ PureLink™ RNA Mini kit (12-183-018A). Briefly,
444 1 µg of RNA was treated with DNase I (Thermo Scientific, EN0521) and retro-transcribed using the
445 High-Capacity cDNA Reverse Transcription Kit (Applied Biosystems, 4368814). Semi-quantitative PCR
446 was performed with the resulting cDNA using the LightCycler 480 SYBR Green I kit (Roche,
447 4707516001) and the primers listed below. The specificity and efficiency of primer pairs were defined
448 prior to their usage.

449

Gene	Specie	Forward primer	Reverse primer	Efficiency
ARHGEF3	Human	5'-cttcgatgtgtgcgtcaa-3'	5'-ttatggagagtttcagcatgg-3'	1.949
LORICRIN		5'-aggttaagacatgaaggatttgcaa-3'	5'-ggcaccgatgggcttagag-3'	2.009
KRT10		5'-tggttcaatgaaaagagcaagga-3'	5'-gggattgtttcaaggccagtt-3'	2.058
GUSB		5'-atggaagaagtggtgcgtag-3'	5'-ccttgtctgctgcatagttaga-3'	1.931
RPLP0		5'-acaaccctgaagtgcttgata-3'	5'-gactcgtttgtacccgttga-3'	1.968

450

451 **Lentiviral production and infection**

452 Envelope vector pPAX2 and packaging vector pVSV-G were kindly gifted by Amélie Fradet-Turcotte
453 (Laval University, Quebec, Canada). The sequence of Arhgef3 isoform 3 with no ATG was cloned into a
454 pCW57.1-3XFLAG pDEST vector. Lentiviral particles were produced by transfecting HEK293T cells
455 with pPAX2, pVSV-G and 3XFLAG-ARHGEF3. Viral particles were collected after 48 hours of
456 transfection and used to infect Ker-CT cells. Cells were selected with 1µg/ml puromycin and 3XFLAG-
457 ARHGEF3 expression was induced using 50 ng/ml hygromycin B (BioBasic, BS725).

458

459 **Western blotting**

460 Proteins were extracted from cells in RIPA lysis buffer containing 10 mM Tris-HCl pH 8.0, 1mM EDTA,
461 0.5mM EGTA, 1% Triton X-100, 0.1% sodium deoxycholate, 0.1% SDS, 140 mM NaCl, and
462 supplemented with freshly added 1X proteases inhibitors (Roche, cOmplete EDTA-free Protease
463 Inhibitor Cocktail, 11836170001). Lysates were centrifuged at 15,000 RPM for 15 minutes to remove
464 debris. Samples were run on 8% polyacrylamide gel. Nitrocellulose membranes (Cytiva, 10600002) were
465 incubated overnight with the following antibodies: FLAG (Sigma, F1804; 1:1,000), ARHGEF3
466 (ThermoFisher, PA5-30608; 1:5,000), Keratin 10 (BioLegend, 905403; 1:10,000), GAPDH
467 (ThermoFisher, 39-8600; 1:10,000), E-cadherin (BD Biosciences, 610181; 1:500) and P-cadherin (R&D,

468 AF761; 1:400). Secondary antibodies used were anti-mouse HRP (Millipore Sigma, A9044; 1:15,000),
469 anti-rabbit HRP (Jackson Immunoresearch, 111-035-144; 1:15,000) and anti-goat HRP (Jackson
470 Immunoresearch, 305-035-003; 1:15,000).
471
472 **Statistical Analysis**
473 Statistical analyses were all performed with Prism 8 (GraphPad Software) unless stated otherwise. In all
474 analysis, experiments were made independently for each pair of sibling embryos (*Arhgef3*$^{+/+}$ and
475 *Arhgef3*$^{-/-}$; sex as a biological variable was not considered given the embryonic nature of the analysis).
476 For proliferation rate based on EdU^{+} cells for both basal layer and hair follicle analysis, the total number
477 of EdU^{+} P-cadherin^{+} cells per embryo was normalized with the total number of P-cadherin^{+} cells (based
478 on DAPI staining). The difference between proliferation rates was assessed with a two-tailed Mann-
479 Whitney test with α=0.05 since there were only n=5 individuals per sample.
480 For both skin thickness, peg length and placode area, measurements were made multiple times on n=5
481 individuals per genotype and the difference between these two groups was assessed with a two-tailed
482 nested t-test with α=0.05. Nested t-test permits to adjust the well-known t-test for the multiple
483 measurements made in the same individual.
484 For the average number of hair placodes, germs, and pegs per 1 mm^2 region of back skin, a two-way
485 ANOVA was performed followed by multiple comparisons for each hair follicle stage with n=5 embryos
486 per genotype. Sidak's correction was applied to adjust for those multiple comparisons and adjusted P
487 values are reported (with starting α=0.05).
488 For the relative expression of mRNA, a two-way ANOVA was performed on the transformed data of
489 n=3 independent experiments (each with 3 technical replicates). Multiples comparisons were made with
490 Dunnett's correction to assess the difference between each differentiation time compared to proliferation
491 state and adjusted P value are reported (with starting α=0.05).
492 For hair follicle angle as well as for CELSR1 angle, the circular mean was calculated. In brief, all
493 individual angle measures (θ) were transformed to radians and then in a (x, y) format using this formula:
494 (x, y) where x=sinθ and y=cosθ. The sum of those (x, y) coordinates was calculated and reverted to
495 degrees to give the circular mean=deg(tan(Σ(x), Σ(y))). For both datasets, a Watson-Wheeler test was
496 performed with R Studio (2024.04.2) to compare the distribution of the angles between *Arhgef3*$^{+/+}$ and
497 *Arhgef3*$^{-/-}$ animals. This non-parametric test (for which the null hypothesis is that the two samples of
498 angles come from the same population) was chosen to consider the fact that the angles measured could
499 never be fully circular due to the nature of the measurement. When many measures are taken, the Watson-

Wheeler test for homogeneity of angles is approximately a Chi-square test with 2 degrees of freedom. For hair follicle angle, a total of 10 embryos (5 per genotype) were analyzed from 5 independent experiments (hair follicles analyzed: *Arhgef3*$^{+/+}$ = 549; *Arhgef3*$^{-/-}$ = 545). For CELSR1 domains angle, a total of 6 embryos (3 per genotype) were analyzed from 3 independent experiments (cells analyzed: *Arhgef3*$^{+/+}$ =577; *Arhgef3*$^{-/-}$ = 540). All ties were randomly broken apart, giving a higher uncertainty on the P values obtained. To provide more information on that variability, we proceeded to 20 iterations of the test and reported the mean P value ± standard deviation (SD). We then performed a two-sided Fisher's exact test on the same datasets to assess the difference in the number of straight hair follicle (]80.0°-90.0]) and the number of polarized cells (visually determined with opposing CELSR1 domains), respectively.

ACKNOWLEDGEMENTS

We thank Steve Bilodeau for discussions; Patrick Laprise and Kathie Cockburn for the critical reading of the manuscript; Dr. Elaine Fuchs for the CELSR1 antibody; Carl St-Pierre from the "*Unité d'imagerie cellulaire, axe Oncologie – site de l'Hôtel-Dieu de Québec"* for assistance with microscopy; and the animal health technicians from the CHU de Québec – Université Laval-LOEX research center for mouse colony maintenance and animal care.

COMPETING INTERESTS

The authors declare no competing interests.

FUNDING

M.L. and P.L. receive salary awards from the Fonds de Recherche du Québec – Santé (FRQ-S). This work was funded by an operating grant from the Canadian Institutes of Health Research (CIHR; PJT-178198). J.C. is supported by the National Institutes of Health (R01 GM089771). A.B. is supported by a scholarship from FRQ-S and CIHR. D.I.H. holds a CIHR fellowship. S.G is supported by a scholarship from the Cancer Research Society.

527 **REFERENCES**

528

529 1. Schneider MR, Schmidt-Ullrich R, Paus R. The Hair Follicle as a Dynamic Miniorgan.
530 Vol. 19, Current Biology. 2009.
531 2. Sennett R, Rendl M. Mesenchymal-epithelial interactions during hair follicle
532 morphogenesis and cycling. Vol. 23, Seminars in Cell and Developmental Biology.
533 Elsevier Ltd; 2012. p. 917–27.
534 3. Saxena N, Mok KW, Rendl M. An updated classification of hair follicle morphogenesis.
535 Vol. 28, Experimental Dermatology. Blackwell Publishing Ltd; 2019. p. 332–44.
536 4. Biggs LC, Kim CS, Miroshnikova YA, Wickström SA. Mechanical Forces in the Skin:
537 Roles in Tissue Architecture, Stability, and Function. Vol. 140, Journal of Investigative
538 Dermatology. Elsevier B.V.; 2020. p. 284–90.
539 5. Fiore VF, Krajnc M, Quiroz FG, Levorse J, Pasolli HA, Shvartsman SY, et al. Mechanics
540 of a multilayer epithelium instruct tumour architecture and function. Nature.
541 2020;585(7825):433–9.
542 6. Shyer AE, Rodrigues AR, Schroeder GG, Kassianidou E, Kumar S, Harland RM.
543 Emergent cellular self-organization and mechanosensation initiate follicle pattern in the
544 avian skin. Science (1979). 2017;
545 7. Villeneuve C, Hashmi A, Ylivinkka I, Lawson-Keister E, Miroshnikova YA, Pérez-
546 González C, et al. Mechanical forces across compartments coordinate cell shape and fate
547 transitions to generate tissue architecture. Nat Cell Biol. 2024 Feb 1;26(2):207–18.
548 8. Le HQ, Ghatak S, Yeung CYC, Tellkamp F, Günschmann C, Dieterich C, et al.
549 Mechanical regulation of transcription controls Polycomb-mediated gene silencing during
550 lineage commitment. Nat Cell Biol. 2016;
551 9. Miroshnikova YA, Le HQ, Schneider D, Thalheim T, Rübsam M, Bremicker N, et al.
552 Adhesion forces and cortical tension couple cell proliferation and differentiation to drive
553 epidermal stratification. Nat Cell Biol. 2018 Jan 1;20(1):69–80.
554 10. Luxenburg C, Heller E, Pasolli HA, Chai S, Nikolova M, Stokes N, et al. Wdr1-mediated
555 cell shape dynamics and cortical tension are essential for epidermal planar cell polarity.
556 Nat Cell Biol. 2015;17(5):592–604.
557 11. Cohen J, Raviv S, Adir O, Padmanabhan K, Soffer A, Luxenburg C. The Wave complex
558 controls epidermal morphogenesis and proliferation by suppressing Wnt-Sox9 signaling.
559 Journal of Cell Biology. 2019;
560 12. Gonzales KAU, Fuchs E. Skin and Its Regenerative Powers: An Alliance between Stem
561 Cells and Their Niche. Vol. 43, Developmental Cell. 2017. p. 387–401.
562 13. Mikkola ML, Millar SE. The mammary bud as a skin appendage: Unique and shared
563 aspects of development. J Mammary Gland Biol Neoplasia. 2006;
564 14. Ahtiainen L, Lefebvre S, Lindfors PH, Renvoisé E, Shirokova V, Vartiainen MK, et al.
565 Directional Cell Migration, but Not Proliferation, Drives Hair Placode Morphogenesis.
566 Dev Cell. 2014;28(5):588–602.
567 15. Ouspenskaia T, Matos I, Mertz AF, Fiore VF, Fuchs E. WNT-SHH Antagonism Specifies
568 and Expands Stem Cells prior to Niche Formation. Cell. 2016;
569 16. Cetera M, Leybova L, Joyce B, Devenport D. Counter-rotational cell flows drive
570 morphological and cell fate asymmetries in mammalian hair follicles. Nat Cell Biol. 2018;
571 17. Schramek D, Sendoel A, Segal JP, Beronja S, Heller E, Oristian D, et al. Direct in vivo
572 RNAi screen unveils myosin IIa as a tumor suppressor of squamous cell carcinomas.
573 Science (1979). 2014;

574 18. Devenport D. The cell biology of planar cell polarity. Journal of Cell Biology. 2014.
575 19. Devenport D, Fuchs E. Planar polarization in embryonic epidermis orchestrates global
576 asymmetric morphogenesis of hair follicles. Nat Cell Biol. 2008;10(11):1257–68.
577 20. Aw WY, Heck BW, Joyce B, Devenport D. Transient Tissue-Scale Deformation
578 Coordinates Alignment of Planar Cell Polarity Junctions in the Mammalian Skin. Current
579 Biology. 2016;
580 21. Simonson L, Oldham E, Chang H. Overactive Wnt5a signaling disrupts hair follicle
581 polarity during mouse skin development. Development (Cambridge). 2022 Nov
582 1;149(22).
583 22. Chang H, Smallwood PM, Williams J, Nathans J. The spatio-temporal domains of
584 Frizzled6 action in planar polarity control of hair follicle orientation. Dev Biol.
585 2016;409(1):181–93.
586 23. Dong B, Vold S, Olvera-Jaramillo C, Chang H. Functional redundancy of frizzled 3 and
587 frizzled 6 in planar cell polarity control of mouse hair follicles. Development
588 (Cambridge). 2018 Oct 1;145(19).
589 24. Cetera M, Leybova L, Woo FW, Deans M, Devenport D. Planar cell polarity-dependent
590 and independent functions in the emergence of tissue-scale hair follicle patterns. Dev
591 Biol. 2017 Aug 1;428(1):188–203.
592 25. Walck-Shannon E, Hardin J. Cell intercalation from top to bottom. Vol. 15, Nature
593 Reviews Molecular Cell Biology. 2014. p. 34–48.
594 26. Panousopoulou E, Green JBA. Invagination of Ectodermal Placodes Is Driven by Cell
595 Intercalation-Mediated Contraction of the Suprabasal Tissue Canopy. PLoS Biol. 2016
596 Mar 9;14(3).
597 27. Müller-Röver S, Tokura Y, Welker P, Furukawa F, Wakita H, Takigawa M, et al. E- and P-
598 cadherin expression during murine hair follicle morphogenesis and cycling. Exp
599 Dermatol. 1999;8(4):237–46.
600 28. Hirai Y, Nose A, Kobayashi S, Takeichi M. Expression and role of E- and P-cadherin
601 adhesion molecules in embryonic histogenesis. I. Lung epithelial morphogenesis.
602 Development. 1989;
603 29. Rhee H, Polak L, Fuchs E. Lhx2 maintains stem cell character in hair follicles. Science
604 (1979). 2006;
605 30. Jamora C, DasGupta R, Kocieniewski P, Fuchs E. Links between signal transduction,
606 transcription and adhesion in epithelial bud development. Nature. 2003;
607 31. Beronja S, Livshits G, Williams S, Fuchs E. Rapid functional dissection of genetic
608 networks via tissue-specific transduction and RNAi in mouse embryos. Nat Med. 2010;
609 32. Laurin M, Gomez NC, Levorse J, Sendoel A, Sribour M, Fuchs E. An RNAi screen
610 unravels the complexities of rho GTPase networks in skin morphogenesis. Elife. 2019;8.
611 33. Hodge RG, Ridley AJ. Regulating Rho GTPases and their regulators. Vol. 17, Nature
612 Reviews Molecular Cell Biology. 2016. p. 496–510.
613 34. Pecora A, Laprise J, Dahmene M, Laurin M. Skin cancers and the contribution of rho
614 GTPase signaling networks to their progression. Vol. 13, Cancers. 2021.
615 35. Dahmene M, Quirion L, Laurin M. High Throughput strategies Aimed at Closing the GAP
616 in Our Knowledge of Rho GTPase Signaling. Vol. 9, Cells. 2020.
617 36. Arthur WT, Ellerbroek SM, Der CJ, Burridge K, Wennerberg K. XPLN, a guanine
618 nucleotide exchange factor for RhoA and RhoB, but not RhoC. Journal of Biological
619 Chemistry. 2002;
620 37. Thiesen S, Kübart S, Ropers HH, Nothwang HG. Isolation of two novel human RhoGEFs,
621 ARHGEF3 and ARHGEF4, in 3p13-21 and 2q22. Biochem Biophys Res Commun. 2000;

38. Khanna N, Fang Y, Yoon MS, Chen J. XPLN is an endogenous inhibitor of mTORC2. Proc Natl Acad Sci U S A. 2013;110(40):15979–84.
39. You JS, Singh N, Reyes-Ordonez A, Khanna N, Bao Z, Zhao H, et al. ARHGEF3 Regulates Skeletal Muscle Regeneration and Strength through Autophagy. Cell Rep. 2021;
40. Zou S, Teixeira AM, Kostadima M, Astle WJ, Radhakrishnan A, Simon LM, et al. SNP in human ARHGEF3 promoter is associated with DNase hypersensitivity, transcript level and platelet function, and Arhgef3 KO mice have increased mean platelet volume. PLoS One. 2017;
41. Zhou F, Ai W, Zhang Y, Hu Q, Gan M, Wang J Bin, et al. ARHGEF3 regulates the stability of ACLY to promote the proliferation of lung cancer. Cell Death Dis. 2022;13(10):1–15.
42. Tomann P, Paus R, Millar SE, Scheidereit C, Schmidt-Ullrich R. Lhx2 is a direct NF-κB target gene that promotes primary hair follicle placode down-growth. Development (Cambridge). 2016;
43. Jacob T, Annusver K, Czarnewski P, Dalessandri T, Kalk C, Levra Levron C, et al. Molecular and spatial landmarks of early mouse skin development. Dev Cell. 2023;58(20):2140-2162.e5.
44. Sennett R, Wang Z, Rezza A, Grisanti L, Roitershtein N, Sicchio C, et al. An Integrated Transcriptome Atlas of Embryonic Hair Follicle Progenitors, Their Niche, and the Developing Skin. Dev Cell. 2015;
45. Sulic AM, Das Roy R, Papagno V, Lan Q, Saikkonen R, Jernvall J, et al. Transcriptomic landscape of early hair follicle and epidermal development. Cell Rep. 2023;42(6):112643.
46. Rezza A, Wang Z, Sennett R, Qiao W, Wang D, Heitman N, et al. Signaling Networks among Stem Cell Precursors, Transit-Amplifying Progenitors, and their Niche in Developing Hair Follicles. Cell Rep. 2016;
47. Liu TH, Zheng F, Cai MY, Guo L, Lin HX, Chen JW, et al. The putative tumor activator ARHGEF3 promotes nasopharyngeal carcinoma cell pathogenesis by inhibiting cellular apoptosis. Oncotarget. 2016;7(18):25836–48.
48. Liao L, Qian Z yang, Li X yu, Yang D shun, Lei B jun, Li H jun, et al. Disrupting RhoA activity by blocking Arhgef3 expression mitigates microglia-induced neuroinflammation post spinal cord contusion. J Neuroimmunol. 2021 Oct 15;359.
49. Kamio K, Azuma A, Usuki J, Matsuda K, Inomata M, Nishijima N, et al. XPLN is modulated by HDAC inhibitors and negatively regulates SPARC expression by targeting mTORC2 in human lung fibroblasts. Pulm Pharmacol Ther. 2017;44:61–9.
50. Yoon J, Kumar V, Goutam RS, Kim SC, Park S, Lee U, et al. Bmp signal gradient modulates convergent cell movement via Xarhgef3.2 during gastrulation of Xenopus embryos. Cells. 2022 Jan 1;11(1).
51. Popov IK, Kwon T, Crossman DK, Crowley MR, Wallingford JB, Chang C. Identification of new regulators of embryonic patterning and morphogenesis in Xenopus gastrulae by RNA sequencing. Dev Biol. 2017 Jun 15;426(2):429–41.
52. Qin K, Yu M, Fan J, Wang H, Zhao P, Zhao G, et al. Canonical and noncanonical Wnt signaling: Multilayered mediators, signaling mechanisms and major signaling crosstalk. Vol. 11, Genes and Diseases. KeAi Communications Co.; 2024. p. 103–34.
53. Jamora C, Lee P, Kocieniewski P, Azhar M, Hosokawa R, Chai Y, et al. A signaling pathway involving TGF-β2 and snail in hair follicle morphogenesis. PLoS Biol. 2005 Jan;3(1).

670 **FIGURE LEGENDS**

671

672 **Figure 1. ARHGEF3 is expressed in the developing skin.** (A) Gene-level RNA expression of *Arhgef3*
673 in the hair placode and the epidermis using the *Hair-GEL* and *Sulic et al*. datasets, shown as mean
674 fragments per kilobase per million (FPKMs) ± SEM (n=9). (B) Expression of *Arhgef3* transcript variants
675 in the placode and the epidermis using the *Hair-GEL* and *Sulic et al.* datasets, shown as mean FPKMs ±
676 SEM (n=9) (C) RNAscope® *in situ* hybridization (ISH) targeting *Arhgef3* mRNA (magenta) in the
677 epidermis. Upregulation of transcript levels in the hair placode can be observed in the mouse skin tissue
678 at E18.5 by the number of probe's dots in this compartment. *Polr2a* mRNA is ubiquitously expressed in
679 cells and used as a positive control. Scale bars: 25 µm. DAPI is used to label cell nuclei. Dotted green
680 line is used to delimit the epidermis and hair follicles from the dermis.

681

682 **Figure 2. ARHGEF3 is not required for skin barrier formation.** (A) EdU and P-cadherin
683 immunofluorescence on E18.5 back skin sections. (B) Graph displays the quantification of the average
684 percentage of basal (P-cadherin^{+}) EdU^{+} cells ± SEM. Statistical analyses were performed using a two-
685 tailed Mann-Whitney test, P value=0.4206, n=5 embryos per genotype from 5 litters and the experiment
686 was independently performed 5 times. (C) P-cadherin and Keratin 10 immunofluorescence on E18.5
687 sagittal back skin sections. (D) Graph displays the average skin thickness ± SEM. Statistical analyses
688 were performed using a two-tailed nested t-test, P value=0.5489, n=5 embryos (25, 30, 30, 15 and 15
689 measures) per genotype from 5 litters and the experiment was independently performed 5 times. (E)
690 LORICRIN, (F) Filaggrin and P-cadherin immunofluorescence on E18.5 back skin sections.
691 Representation of n=4 embryos. Proper expression of LORICRIN and Filaggrin is observed in both
692 *Arhgef3*$^{+/+}$ and *Arhgef3*$^{-/-}$ animals. (G) Barrier assays on E16.5, E17.5 and E18.5 *Arhgef3*$^{+/+}$ and *Arhgef3*$^{-}$
693 $^{/-}$ mouse embryos. Representation of n=3. Scale bars: 25 µm. DAPI is used to label cell nuclei. Dotted
694 white line is used to delimit the epidermis and hair follicle from the dermis.

695

696 **Figure 3. ARHGEF3 is required for proper hair follicle morphogenesis.** (A) Maximum intensity Z-
697 projections of P-cadherin whole-mount immunofluorescence of E16.5 back skin. Scale bars: 100 µm.
698 The anterior – posterior axis of the embryo is indicated. (B) Graph displays the average number of hair
699 placodes, germs, and pegs from the staggered hair follicle waves per 1 mm^2 region of back skin ± SEM.
700 Statistical analyses were performed using two-way ANOVA followed by multiple comparisons (with
701 Sidak's correction) between *Arhgef3*$^{+/+}$ and *Arhgef3*$^{-/-}$ conditions for each hair follicle stage. All

702 comparisons were not significant (adjusted P values: placode = 0.5052; germ = 0.9967; peg = 0.9911),
703 n=5 embryos per genotype from 5 litters and the experiment was independently performed 5 times. (C)
704 EdU and P-cadherin immunofluorescence of E18.5 back skin sections. Scale bars: 25 µm. DAPI is used
705 to label cell nuclei. Dotted white line is used to delimit the epidermis and hair follicle from the dermis.
706 (D) Graph displays the average percentage of EdU^+ hair follicle cells ± SEM. Statistical analyses were
707 performed using a two-tailed Mann-Whitney test, P value=0.0312, n=5 embryos per genotype from 5
708 litters and the experiment was independently performed 5 times (hair follicles analyzed: *Arhgef3*$^{+/+}$ =
709 255; *Arhgef3*$^{-/-}$ = 205). (E) Graph displays the average length of hair follicle (pegs at E18.5) per embryo
710 ± SEM. Statistical analyses were performed using a two-tailed nested t-test, P value=0.6359, n=5
711 embryos per genotype from 5 litters and the experiment was independently performed 5 times (peg
712 analyzed : *Arhgef3*$^{+/+}$ = 23, 37, 19, 65, 71; *Arhgef3*$^{-/-}$ = 34, 39, 25, 52, 42). (F) P-cadherin
713 immunofluorescence of E18.5 back skin. Highlighted is the strategy used to measure the angle between
714 the basement membrane and developing hair follicle. Scale bars: 25 µm. (G) Rose plot displays the
715 frequency of hair follicle angle (hair germ and peg) calculated in E with 10° bins. Dashed green line
716 points out the circular mean (*Arhgef3*$^{+/+}$ = 62.77°; *Arhgef3*$^{-/-}$ = 67.40°). Statistical analyses to compare
717 the distribution of angles were performed using Watson-Wheeler test for homogeneity of angles which,
718 with many measurements, is approximately a Chi-square test with 2 degrees of freedom. This test
719 reported 618 ties that were broken apart randomly. Hence, we proceeded to 20 iterations of the test that
720 gave closely related P values: mean P value of iterations = 0.0208495±0.00023 (SD). To assess the
721 difference in the frequency of straight hair follicles (striped bins,]80.0°-90.0°[ ) statistical analysis were
722 performed using a two-sided Fisher's exact test, P value<0.0001, n=5 embryos per genotype from 5 litters
723 and the experiment was independently performed 5 times (hair follicles analyzed: *Arhgef3*$^{+/+}$ = 549;
724 *Arhgef3*$^{-/-}$ = 545).
725
726 **Figure 4. ARHGEF3 is not required to establish CELSR1 planar polarized domain in the**
727 **epidermis.** (A) CELSR1 and E-cadherin whole-mount immunofluorescence of E15.5 back skin. Scale
728 bars: 25 µm. (B) Graph displays the average percentage of planar polarized cells ± SEM. Statistical
729 analyses were performed using a two-sided Fisher's exact test, P value=0.1403, n=3 embryos per
730 genotype from 3 litters and the experiments were independently performed (cells analyzed: *Arhgef3*$^{+/+}$
731 =1473; *Arhgef3*$^{-/-}$ = 1450). (C) Rose plots display the orientation of the opposing CELSR1 domains in
732 the epidermal cells, 90° being perfectly aligned with the anterior-posterior axis of the tissue (bins: 15°).
733 Dashed green lines point out the circular mean (*Arhgef3*$^{+/+}$ = 90.91°; *Arhgef3*$^{-/-}$ = 88.97°). Statistical

734 analyses to compare the distribution of angles were performed using Watson-Wheeler test for
735 homogeneity of angles which, with a large number of measurements, is approximately a Chi-square test
736 with 2 degrees of freedom. This test reported 646 ties that were broken apart randomly. Hence, we
737 proceeded to 20 iterations of the test that gave closely related P values: mean P value of iterations =
738 0.7387±0.01286 (SD), n=3 embryos per genotype from 3 litters and the experiment was independently
739 performed 3 times (cells analyzed: *Arhgef3*$^{+/+}$ =577; *Arhgef3*$^{-/-}$ = 540).
740
741 **Figure 5. ARHGEF3 overexpression promotes the accumulation of P-cadherin at cell-cell**
742 **junctions**. (A) RT-qPCR analysis in proliferating (0) and differentiating Ker-CT (2, 3 and 7 days)
743 showing the normalized expression of *ARHGEF3* mRNA on a log10 scale ± SEM. Proper differentiation
744 of the keratinocytes was assessed using *KRT10* (Keratin 10) and *LORICRIN* mRNA expression (± SEM).
745 Statistical analyses were performed using a two-way ANOVA followed by multiple comparisons with
746 Dunnett's correction to assess the difference between each differentiation time compared to proliferation
747 state (D0), adjusted P value <0.0001, n=3 independent experiments, each with 3 technical replicates. (B)
748 Western blot analysis for ARHGEF3, FLAG and GAPDH (loading control) showing the overexpression
749 of 3xFLAG-ARHGEF3 in the transduced, doxycycline-treated cells. (C) FLAG and F-actin (Phalloidin)
750 immunofluorescence on proliferating (without Ca^{2+}; no cell-cell junctions) and differentiating (with Ca^{2+};
751 with cell-cell junctions) keratinocytes. Scale bars: 10 µm. DAPI is used to label cell nuclei. (D) E-
752 cadherin and FLAG immunofluorescence of keratinocytes grown for 48 hours in the presence of Ca^{2+}.
753 Scale bars: 10 µm. DAPI is used to label cell nuclei. Dotted yellow lines show the exact x slice where
754 orthogonal views (y, z) were taken. (E) P-cadherin and FLAG immunofluorescence on keratinocytes
755 grown for 24 hours in the presence of Ca^{2+}. Scale bars: 10 µm. DAPI is used to label cell nuclei. (F)
756 Western blot analysis for FLAG, E-cadherin, P-cadherin and GAPDH (loading control) in keratinocytes
757 grown in proliferating and differentiating conditions with or without doxycycline as indicated.
758
759 **Figure 6. ARHGEF3 promotes placode compaction.** (A) E-cadherin, FLAG, and F-actin (Phalloidin)
760 immunofluorescence on keratinocytes grown for 24 hours in the presence of Ca^{2+} to allow cell-cell
761 junctions to form. Scale bars: 10 µm. DAPI is used to label cell nuclei. Dotted yellow lines show the
762 exact x slice where orthogonal views (y, z) were taken. (B) P-cadherin whole-mount immunofluorescence
763 of E16.5 back skin. Scale bars: 10 µm. (C) Graph displays the average placode cell area ± SEM. Statistical
764 analyses were performed using a two-tailed nested t-test, P value=0.0036, n=5 embryos per genotype

765 from 5 litters and the experiment was independently performed 5 times (number of placodes analyzed:
766 *Arhgef3*$^{+/+}$ = 43, 29, 25, 45, 30; *Arhgef3*$^{-/-}$ = 25, 48, 36, 44, 17).

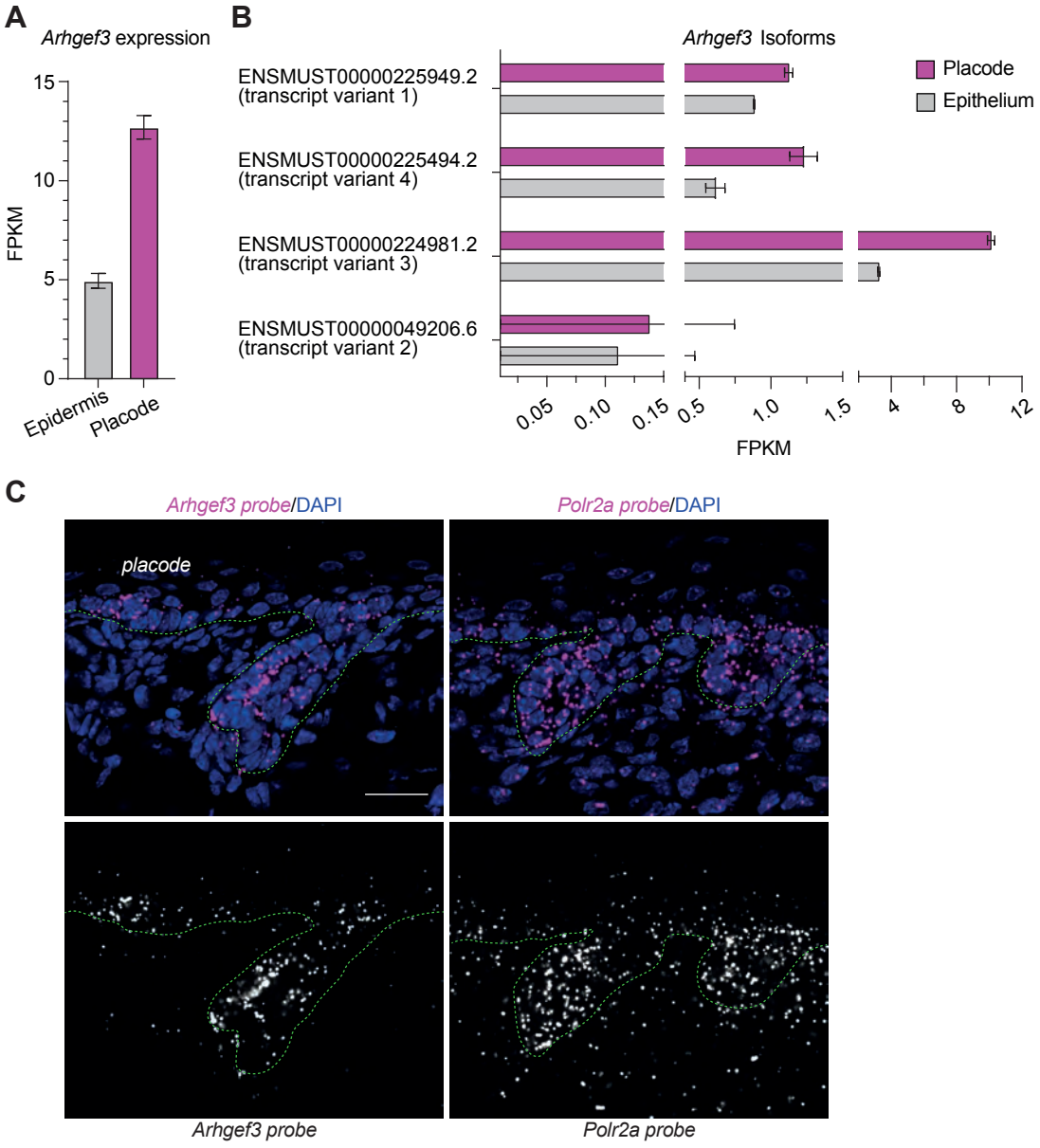

Kalyanakrishnan, et al. Fig. 1

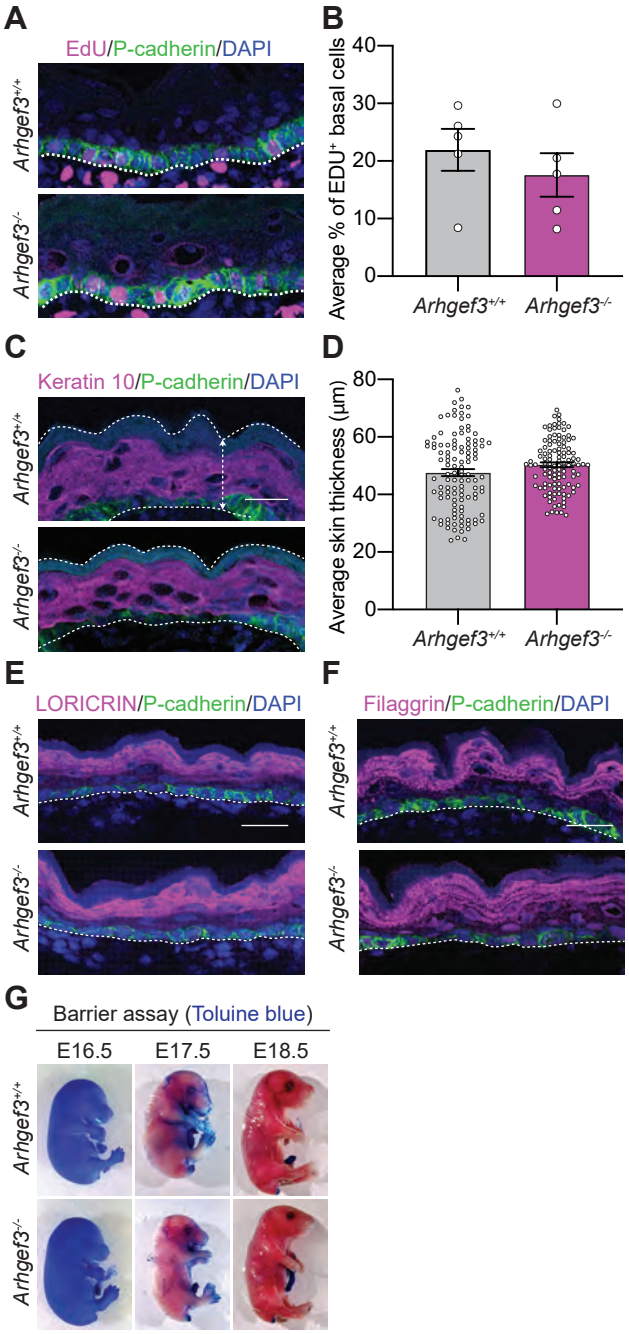

Kalyanakrishnan, et al. Fig. 2

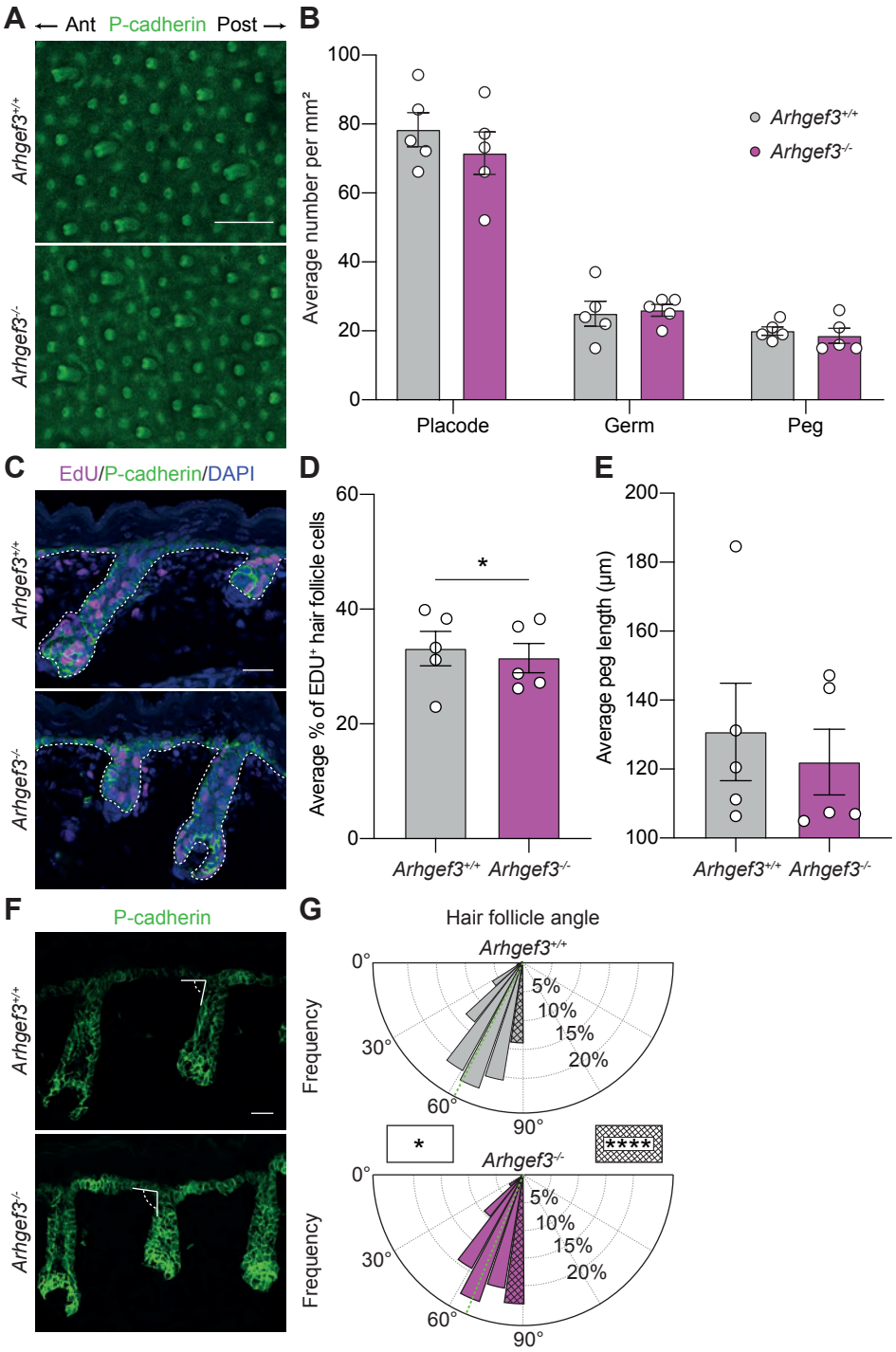

Kalyanakrishnan, et al. Fig. 3

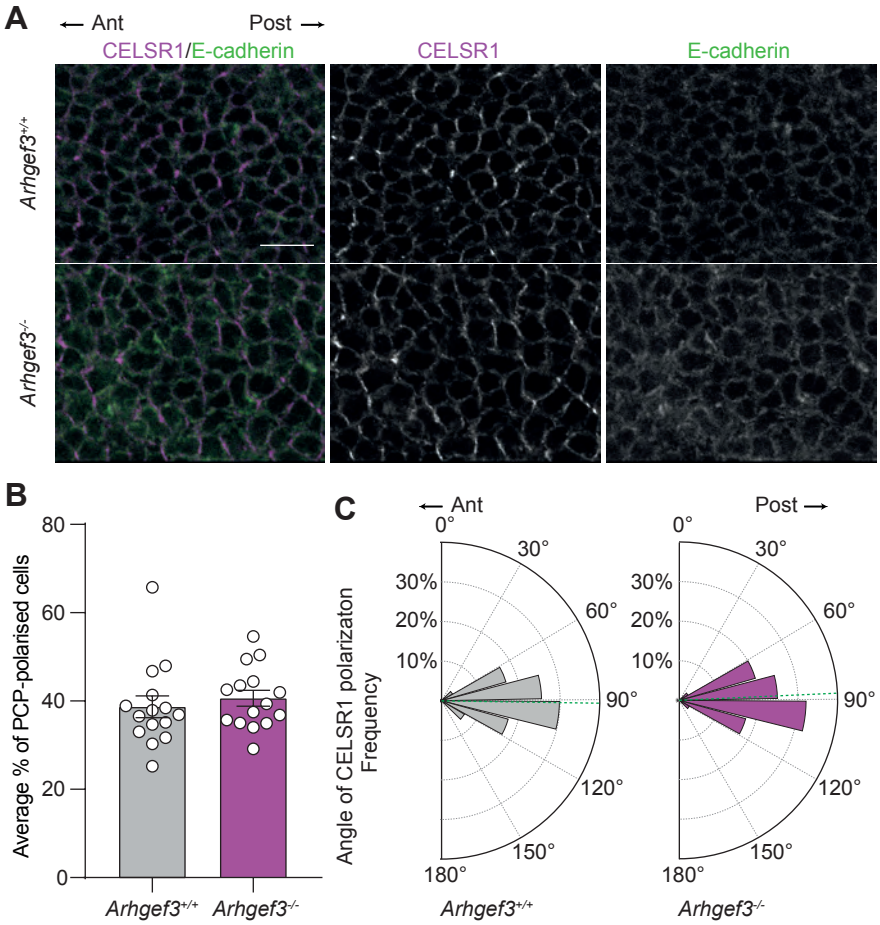

Kalyanakrishnan, et al. Fig. 4

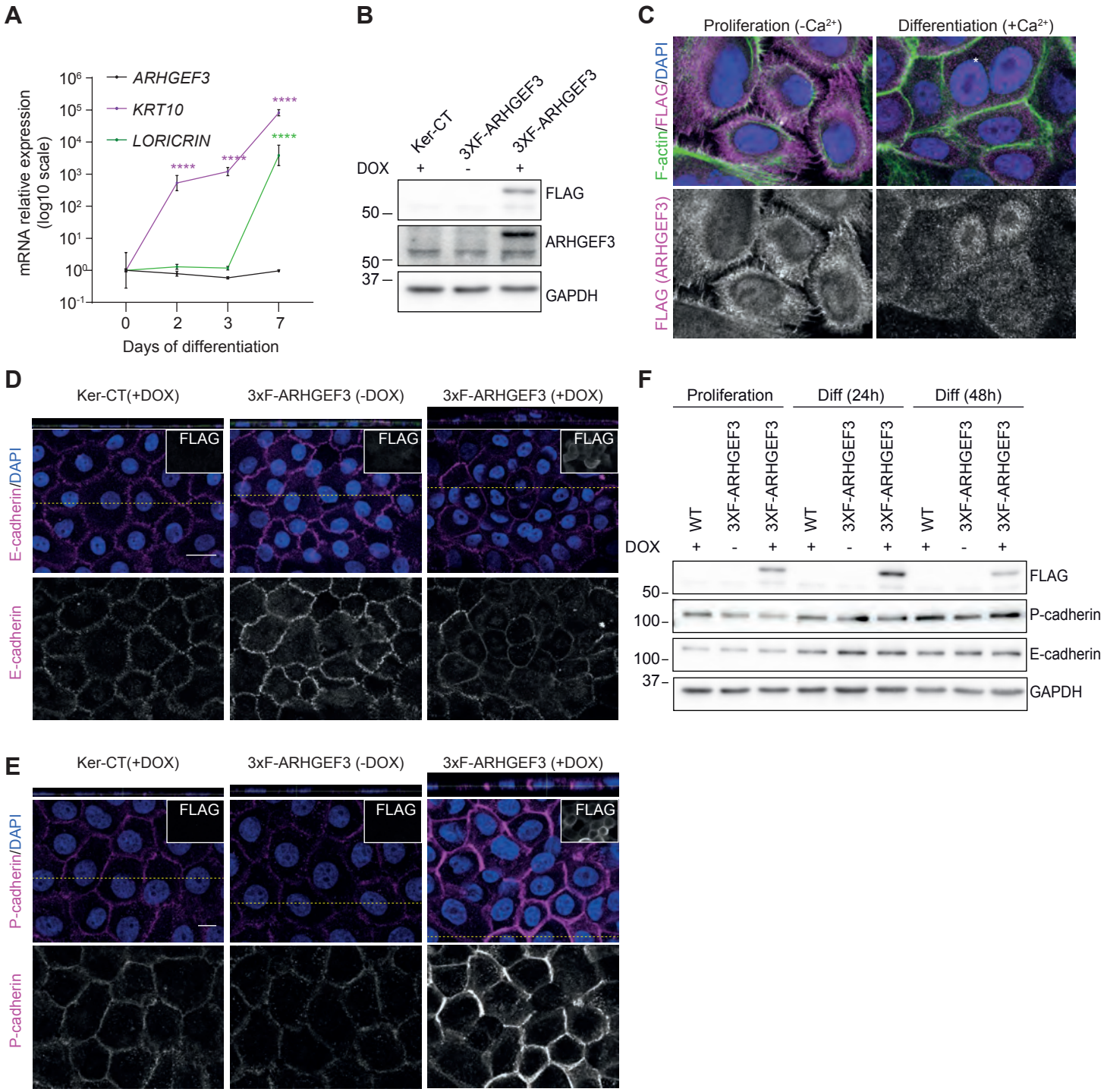

Kalyanakrishnan, et al. Fig. 5

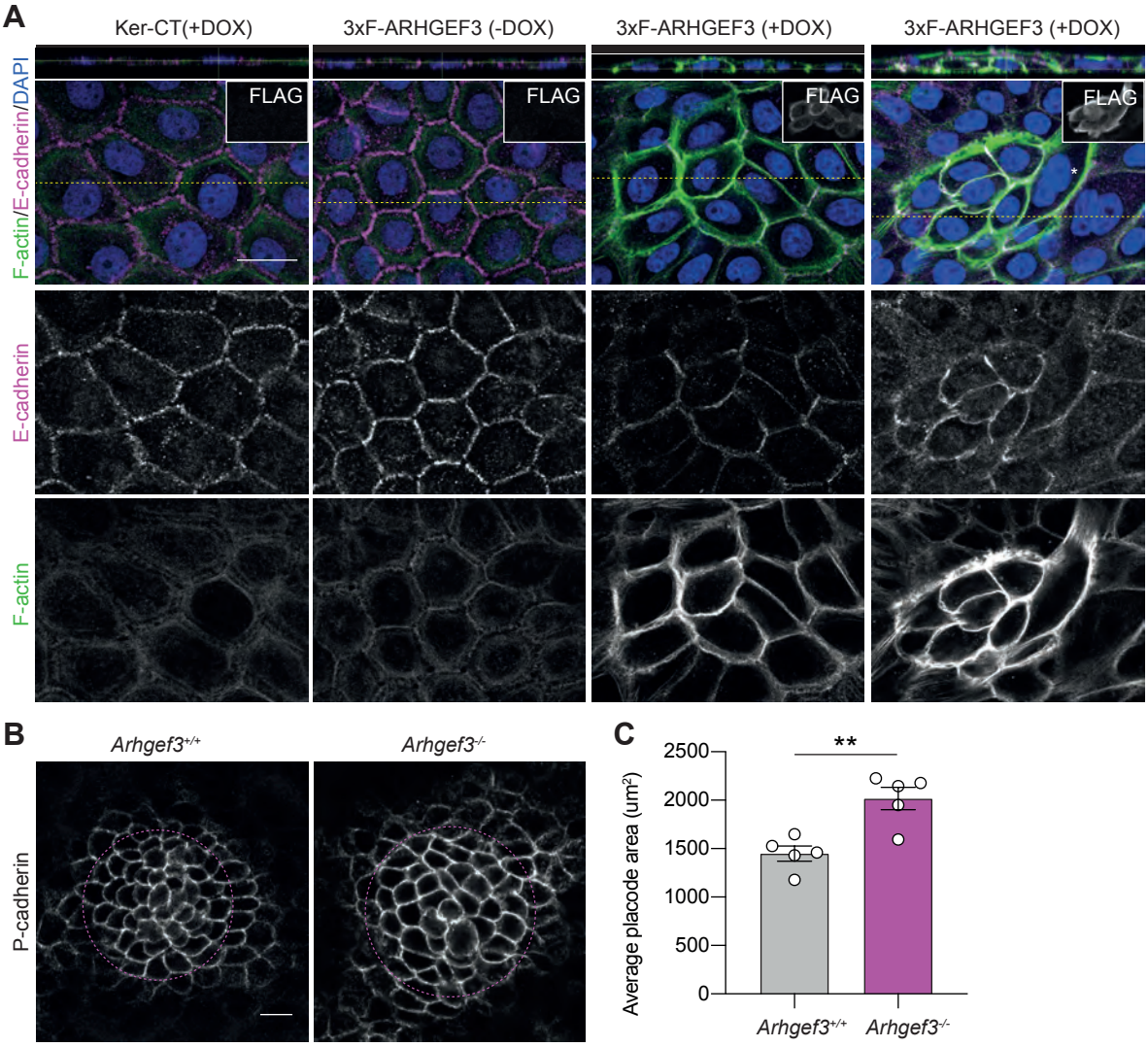

Kalyanakrishnan, et al. Fig. 6